Signal formation in amorphous-Se-based x-ray detectors

E. Fourkal,[2] M. Lachaine,[1,2] and B. G. Fallone[1]
[1]*Medical Physics, Cross Cancer Institute, University of Alberta, 11560 University Avenue, Edmonton, Alberta T6G 1Z2, Canada*
[2]*Physics Department, McGill University, Montreal, Canada*

(Received 15 December 2000; revised manuscript received 24 January 2001; published 16 April 2001)

The present paper addresses the problem of charge creation by x rays in amorphous selenium (a-Se) and the subsequent transport and recombination of these charges. X-ray detectors based on a-Se are under study in medical imaging for diagnostic purposes (keV energy range) and for the verification of radiotherapy treatments (MeV energy range). A quantitative theory is developed that includes collective and single electron-hole pair excitations by the passing electron. This theory is incorporated into a Monte Carlo code to calculate track structures in a-Se. The initial positions of the electron-hole pairs along the track structures are used to study the kinetics of recombination versus incident x-ray energy and applied electric field. The experimentally observed energy dependence of recombination is attributed to a spur size that is dependent on the velocity of the ionizing electrons. Our theory and simulations agree with available experimental data in the energy range from 20 keV to 10 MeV.

DOI: 10.1103/PhysRevB.63.195204 PACS number(s): 71.55.Jv, 71.45.−d, 87.15.Aa

I. INTRODUCTION

There has recently been renewed interest in the use of amorphous selenium (a-Se) based detectors in the field of medical imaging.[1] In these detectors, x-rays are converted directly into charges that are collected at the a-Se surface through the use of an applied electric field. Various techniques have been developed to collect the charges to form a two-dimensional image,[2,3] the most promising being active matrix flat-panel imagers (AMFPI's).

Current research in a-Se-based detectors has involved x rays in the keV energy range for diagnostic purposes and in the MeV range for the verification of radiotherapy treatments.[4–6] The latter modality requires the use of a metal plate above the detector equivalent to about 1 mm of copper to preferentially attenuate scattered radiation originating from the patient, which is typically of lower energy than the primary beam. Since high-energy photons have a small interaction probability with the thin a-Se layers used, the metal plate is also used to increase the detector efficiency by converting high-energy photons into ionizing electrons that subsequently deposit their energy in the a-Se layer.

The average energy required to create an electron-hole pair by ionizing radiation in a-Se, W_0, has been calculated to be approximately 4–7 eV.[7] Experimentally, however, the quantity that is measured is $W_{\pm}$, the energy required to create a *detectable* pair. The latter differs from the former due to recombination and trapping of charges and is related by[8]

$$W_{\pm}=\frac{W_0}{\eta}, \tag{1}$$

where the *escape efficiency* η is defined as the fraction of electron-hole pairs that escape recombination or trapping. Although W_0 is not expected to vary with either electric field or incident photon energy, experimentally measured values of $W_{\pm}$ are dependent on both quantities. The electric field dependence is due to the fact that more pairs will escape recombination as the electric field is increased. The dependence on photon energy, on the other hand, is not well understood.[7,8] A qualitative description has been offered by Mah *et al.*[9] in terms of a simple microdosimetric mechanism. They suggest that the high-energy electrons generated by the incident photons deposit their energy in discrete *spurs*, a concept first introduced in radiation chemistry.[10] The spurs consist of charge clouds created by inelastic collisions with outer atomic shells, which typically occur at the resonant energies of these shells, which has been estimated to lie between 20 eV and 80 eV.[9] In this simple model the spur size is assumed to be independent of the energy of the ionizing electron. At low photon energies, the mean free path between spurs is assumed to be smaller than the spur size, so that the pairs are formed in a column surrounding the ionizing electron track, resulting in a large amount of recombination. As the energy increases, the spurs are formed farther apart resulting in decreased recombination. At megavoltage energies, the spurs are assumed to be isolated from each other so that the amount of recombination is no longer dependent on the incident energy, a fact which has been observed experimentally.

It is clear from the model of Mah *et al.* that the recombination depends on the electron track structure in a-Se. Track structures are of interest in other fields such as radiation chemistry and radiation biology.[11] In a previous work[12,13] we have developed cross sections for use in a Monte Carlo simulation code to produce track structures in the energy range from 40 keV to 140 keV. We have subsequently studied the kinetics of electron-hole pairs produced along the tracks to quantitatively predict the escape efficiency η. Our results have shown good agreement within the energy range studied. In this work, to study the signal formation over a wider range of energies, we reexamine the theory of the elementary processes that occur during the interaction of the photon/electron shower with a-Se. Specifically, we include the plasma wave excitation and its subsequent decay into multiple electron-hole pairs. We also address the question of spur size and the number of charges in a spur as a function of photon energy. We include these effects into the transport code to investigate the dependence of $W_{\pm}$ on both the photon energy and the applied electric field.

II. THEORETICAL DESCRIPTION OF CHARGE FORMATION IN *a*-Se

As an electron traverses a medium, it may undergo elastic, radiative (bremsstrahlung), and inelastic interactions. We focus on the latter since it is the main mechanism for the creation of electron-hole pairs. Inner-shell electrons are tightly bound to the ion core and thus inner collisions with these electrons can be reasonably approximated by known cross sections for isolated atoms. Inelastic collisions with outer-shell electrons, on the other hand, typically involve low-energy transfers and are strongly influenced by the structure of the medium. The cross sections can be calculated in the first Born approximation by the equation[14–16]

$$\frac{d\sigma}{d\hbar\omega}=\frac{2e^2}{h^2Nv^2\epsilon_0}\int_{\hbar q_-}^{\hbar q_+}\frac{dq}{q}\,\mathrm{Im}\left[\frac{-1}{\epsilon(q,\omega)}\right], \tag{2}$$

where N is the neutral atom density, v is the velocity of the incoming electron, $\hbar q$ is the momentum transfer, and $\epsilon(q,\omega)$ is the dielectric response function of the medium under investigation. Equation (2) can be used at relativistic energies as long as $\hbar q/mc \ll 1$. In general, ϵ may be a tensor that depends on the direction of **q**. In this paper it is assumed that the medium is homogeneous and isotropic so that $\epsilon(q,\omega)$ is a scalar quantity that depends only on the magnitude of **q**. The quantities $\hbar q_-$ and $\hbar q_+$ are the minimum and maximum momentum transfers determined from the energy/momentum conservation equations, which ignoring terms of the order $\hbar\omega/mc^2$, are given by

$$\hbar q_-=\sqrt{2m}\left[\sqrt{E(1+E/2mc^2)}-\sqrt{E(1+E/2mc^2)-\hbar\omega(1+E/mc^2)}\right] \tag{3}$$

and

$$\hbar q_+=\sqrt{2m}\left[\sqrt{E(1+E/2mc^2)}+\sqrt{E(1+E/2mc^2)-\hbar\omega(1+E/mc^2)}\right], \tag{4}$$

where E is the incident electron kinetic energy, $\hbar\omega$ is the energy transferred to the medium, and m is the mass of a free electron. The expressions for $\hbar q_\pm$ assume that the energy-momentum transfer relation for the electron moving in the medium is the same as that for a free electron in vacuum, which is consistent with the formalism used to derive Eq. (2).[16] Equations (3) and (4) determine the plane of all possible momentum and energy transfers to the system. These energy and momentum transfers go into excitation of different degrees of freedom of the medium determined by the spectrum of elementary excitations. There is a certain probability that the energy transfer goes into the creation of a single electron-hole pair. This type of excitation can only occur for energy and momentum transfers bound by the two parabolas[17]

$$\hbar\omega(q)-E_g=\frac{\hbar^2q^2}{2m}\pm\frac{\hbar^2qq_F}{m}, \tag{5}$$

where E_g is the energy gap, which for *a*-Se is about 2.3 eV, and $\hbar q_F$ is the Fermi momentum. Figure 1 shows the single electron-hole domain in the (q,ω) plane.

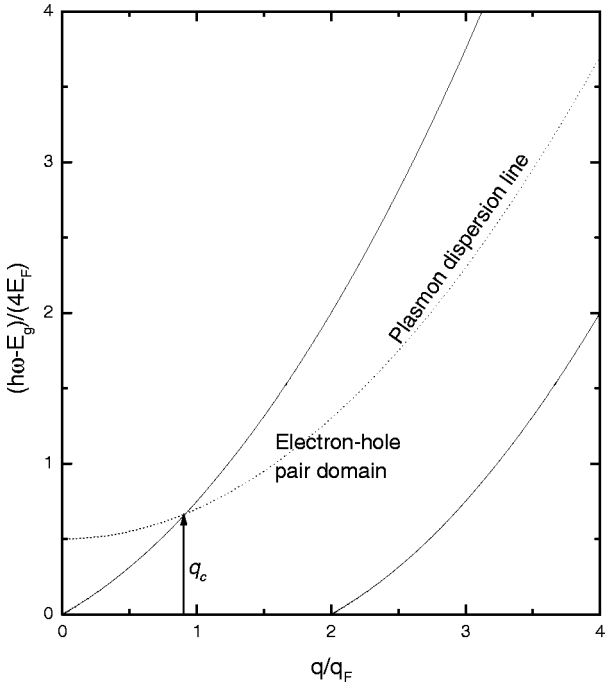

FIG. 1. Spectrum of elementary excitations in the bulk electron gas. The plasmon dispersion line is shown as well as the electron-hole pair domain.

Another possible mechanism that may occur is that the energy transferred by the passing electron may induce collective oscillations of electrons in the medium, i.e., plasma waves. The dispersion relation for these waves is given by[17]

$$\omega_p^2(q)=\omega_{pe}^2+\alpha q^2+\cdots, \tag{6}$$

where $\omega_{pe}=\sqrt{ne^2/\epsilon_0 m}$ is a plasma frequency and $\alpha=\frac{3}{5}v_F^2$. This dispersion line is shown in Fig. 1. It intersects the electron-hole domain at $\hbar q_c$, which is determined by the relation

$$\hbar\omega_p(q_c)=E_g+\frac{\hbar^2q_c^2}{2m}+\frac{\hbar^2q_cq_F}{m}. \tag{7}$$

For $q>q_c$, the plasmon decays into a single-particle excitation state. This implies that in this case, a plasmon lives for a limited time τ after it has been created. If this time is smaller than the characteristic oscillation time of a plasmon ($\sim 2\pi/\omega_{pe}$), then the plasmon cannot exist as a coherent motion of all the electrons in the charge cloud and it will no longer be an observable entity. On the other hand, for the $q<q_c$ regime, the arguments presented above would predict that plasmons are undamped. But experiments indicate that this is not always so, and therefore sources of damping different from the single pair excitations must be invoked in order to explain the observations. Figure 2 shows the experimentally measured optical $(q\sim 0)$ energy loss function $\mathrm{Im}[-1/\epsilon(0,\omega)]$ for *a*-Se (the data have been taken from the paper by Bell and Liang[18]). One can see that the energy loss function is not in the form $\delta(\omega-\omega_{pe})$ as it is for media in which plasma waves are undamped once created.[19] It exhib-

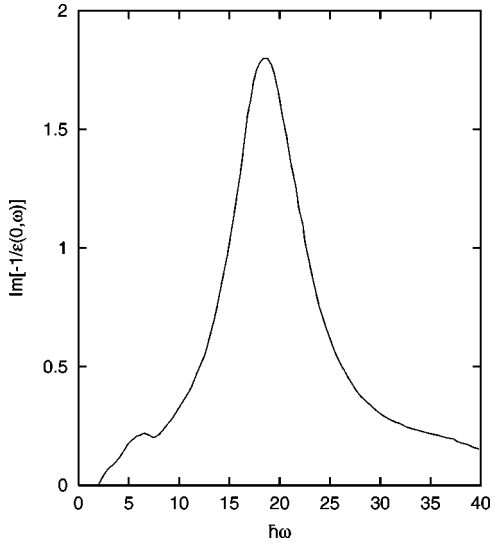

FIG. 2. Optical energy loss function, i.e., the inverse imaginary part of the dielectric function, versus energy transfer.

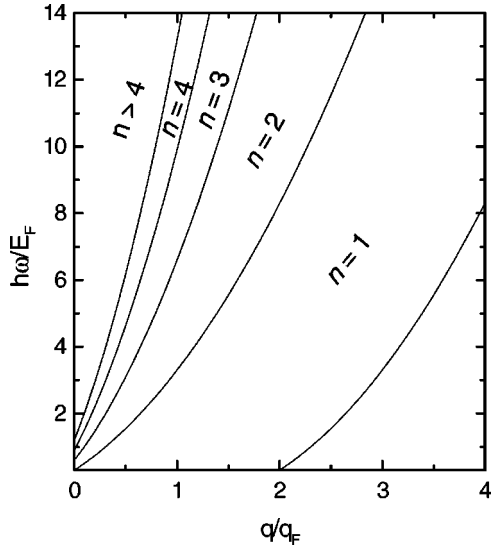

FIG. 3. The *n*-particle excitation domains. Regions from $n=1$ to 4 are explicitly shown on the graph whereas the other regions ($n>4$) are grouped together for clarity.

its a spread about its peak, indicating a finite damping rate ($\gamma \sim \omega_{pe}/2$) and a finite lifetime ($\tau \sim 2/\omega_{pe}$) for plasma waves in this material. This indicates that in *a*-Se energy transfers to collective excitations are not constrained to exist along a single plasmon dispersion line.

One of the sources of plasma damping is the simultaneous excitation of several electron-hole pairs. These multiparticle excitations are no longer confined to lie in the strip of the (q,ω) plane defined by Eq. (5). The possibility that plasma waves decay into several (more than one) electron-hole pairs has also been qualitatively discussed by other authors.[20,21] Another source of damping is the interaction of the electrons with the lattice periodic potential (electron-phonon interaction), resulting in the decay of plasmons into phonons. In the present paper we will concentrate on the effect of plasmon decay into several electron-hole pairs and its manifestation in the studies of charge formation and transport in *a*-Se. Our goal is to obtain the *n*-particle excitation inelastic cross sections and implement them in a Monte Carlo code to study the charge transport.

III. PLASMA WAVE DECAY AND *n*-PARTICLE EXCITATION INELASTIC CROSS SECTIONS

In the physical model presented in this paper, energy transferred in inelastic collisions with outer-shell electrons goes into either the creation of a single electron-hole pair or into the excitation of plasma waves. The plasma waves quickly decay ($\tau \sim 2/\omega_{pe}$) into *n* electron-hole pairs. Since the lifetime of the plasmon is short, the whole picture looks as if the ionizing electron created *n* electron-hole pairs in the vicinity of the interaction point. These pairs constitute a spur. The number *n* of electron-hole pairs in a given spur is a stochastic quantity which can be determined from the *n*-particle excitation inelastic cross sections. To calculate these cross sections one needs to determine the regions of integration in the (q,ω) plane for each individual *n* and integrate Eq. (2) over the regions of interest. The integration regions can be found by considering the relation between the energy and momentum transfer to the system for the case when *n* electrons are excited from the Fermi surface to the conduction band. For a given *n*, the region of allowed excitations is bound by the lines

$$\hbar\omega - nE_g = n\left(\frac{\hbar^2 q^2}{2m} \pm \frac{\hbar^2 q q_F}{m}\right). \tag{8}$$

In Eq. (8) we have assumed that the density of electron states in the Fermi surface is large, so that the initial momenta of the electrons that are subsequently excited into the conduction band are close to the Fermi momentum $\hbar q_F$ (the number of the excited particles is much smaller than the number of the electrons in the Fermi surface). Equation (8) together with Eq. (3) constitutes the domains of the *n*-particle excitations allowed in the system. Figure 3 shows the dispersion relation diagram for the *n*-particle excitation domains. In general, there exists overlapping between different domains, i.e., the single electron-hole domain contains part of the two-particle excitation domain, the two-particle excitation domain contains part of the three-particle excitation, etc. As a first approximation we shall neglect the effect of overlapping in the calculation of the cross sections.

Having identified the integration regions we can proceed to calculate the *n*-particle excitation cross sections. Equation (2) contains the energy loss function $\mathrm{Im}[-1/\epsilon(q,\omega)]$. The optical data, shown in Fig. 2, only gives us the long-wavelength response of the medium. The extension of the energy loss function to $q>0$ from the optical limit is made through the Ashley approximation[22]

$$\mathrm{Im}\left[\frac{-1}{\epsilon(q,\omega)}\right] = \int_0^\infty d\omega' \frac{\omega'}{\omega} \mathrm{Im}\left[\frac{-1}{\epsilon(0,\omega')}\right] \times \delta\left(\omega - \left(\omega' + \frac{\hbar q^2}{2m}\right)\right). \tag{9}$$

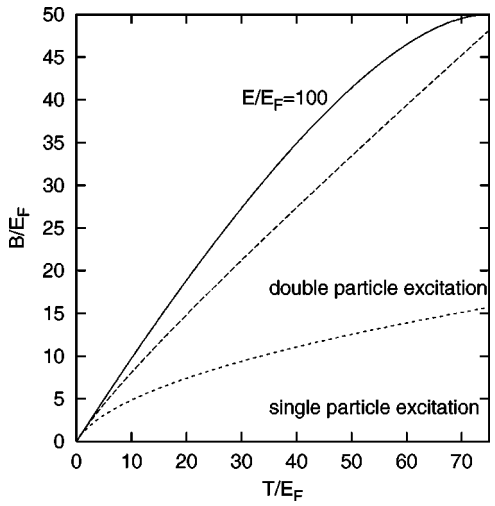

FIG. 4. The n-particle excitation states in the (B,T) plane, for $n=1$ (single particle) and $n=2$ (double particle). The solid line represents the energy-momentum conservation equation [Eqs. (3) and (4)]. The incident electron energy is $E/E_F=100$.

In this approach, the energy loss function $\mathrm{Im}[-1/\epsilon(q,\omega)]$ is treated as being composed of multimodes of a localized plasmon. The q dependence is introduced by extrapolating the optical data for the energy loss function along plasmon dispersion relations.

To simplify the integration in Eq. (2) we map the (q,ω) plane into the (B,T) plane, using the transformation $\hbar^2q^2/2m=T-B$ and $T=\hbar\omega$. The n-particle cumulative inelastic cross section for all energy transfers up to $T'=T$ can be found by substituting Eq. (9) into Eq. (2), leading to

$$\sigma_n(E,T)=\chi\int_0^T dT'\int_0^{B_n} dB f(B)g(T',B), \tag{10}$$

where $\chi=2\pi r_e^2mc^2/\beta^2$, $\beta=v/c$,

$$g(T',B)=\frac{1}{T'(T'-B)}, \tag{11}$$

and $f(B)$ is the dipole oscillator strength distribution, which is related to the energy loss function by

$$f(B)=\frac{2m}{h^2N(e^2/4\pi\epsilon_0)}B\,\mathrm{Im}\left[\frac{-1}{\epsilon(0,B)}\right]. \tag{12}$$

The dipole oscillator strength for energies above the optical data (40 eV) were calculated in Ref. 11. The integration regions for n-particle excitation states in the new (B,T) plane are shown in Fig. 4 and for a given n are defined by the equation

$$B_n=\frac{\sqrt{\beta^2-4\alpha\delta}-\beta}{2\alpha}, \tag{13}$$

where $\alpha=n^2$, $\beta=2n[n(2E_F-E_g-T)+T]$, and $\delta=[T(1-n)-nE_g]^2-4n^2E_FT$.

The domain above the single-particle excitation state (plasmon domain) is split into subdomains for the

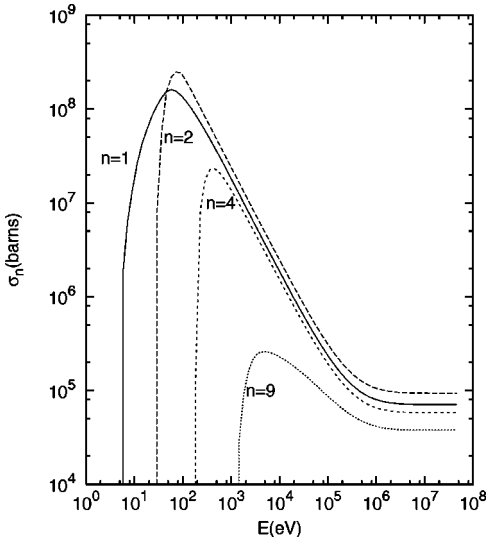

FIG. 5. The calculated n-particle inelastic cross sections versus electron energy.

nth-particle excitation states. Figure 5 shows the n-particle inelastic cross sections. With increasing electron energy, the possibility of creating $n>1$ electron-hole pairs increases. For this reason, since an ionizing electron loses kinetic energy along its path, it has a greater probability of creating more electron-hole pairs in a given spur at the beginning of its track than at the end of its track. The normalized cumulative n-particle cross sections $Y_n(E,T)$ versus energy transfer T, defined as

$$Y_n(E,T)=\frac{\sigma_n(E,T)}{\sigma_n(E)}, \tag{14}$$

where $\sigma_n(E)$ is the total integrated n-particle cross-section, are shown in Fig. 6 for some representative values of n, and for an incident electron energy of 10 keV. We have found that these distributions are relatively insensitive to the electron energy.

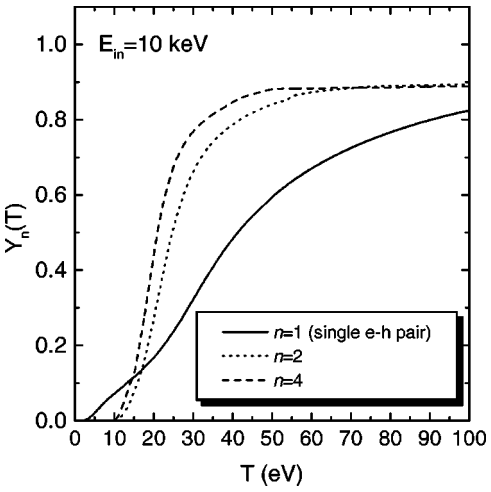

FIG. 6. The calculated n-particle cumulative cross sections as a function of energy transfer. The electron energy is $E=10$ keV.

A question that needs to be addressed is the initial size of a spur. Obviously, energy transferred to the system is not concentrated at one point. One way to approach this problem is as follows.[20] From the viewpoint of the outer atomic electrons, a passing charged particle constitutes an electrical impulse. The duration of the impulse increases with distance r from the particle trajectory as r/v, where v is the charged particle velocity. When the pulse duration becomes much longer than the response time of the bound outer-shell electrons ($\sim 1/\omega_{pe}$), then these electrons follow the electrical field adiabatically. In this case the medium merely polarizes under the influence of the charged particle with negligible energy absorption. The resonant condition $r=v/\omega_{pe}$, *Bohr's adiabatic criterion*,[23] determines the distance of maximum energy deposition from the path of the ionizing particle. This region constitutes the *spur core*, which increases with increasing velocity of the ionizing electron.[24] Qualitatively, this effect would lead to an escape efficiency η that increases with the energy of the ionizing electron.

Electron-hole pairs created in the spur core lose their initial kinetic energy in a thermalization process, after which they are separated by a finite distance r_0. This distance can be estimated for a given initial kinetic energy using the Knights-Davis equation,[25] which assumes that the pair loses its kinetic energy to phonons during a diffusion-dominated thermalization process. We define the *spur size* as the spur core size plus the thermalization distance r_0. In the next section we model the physics described in this section using Monte Carlo techniques to calculate the escape efficiency η and the pair creation energy $W_{\pm}$.

IV. MONTE CARLO SIMULATIONS OF CHARGED-PARTICLE KINETICS

We have previously developed a Monte Carlo code to calculate track structures in a-Se.[13] The code simulates the following interactions: photoelectric, coherent, and incoherent interactions for photons, and elastic and inelastic interactions for electrons. To extend the code to higher energies, we have recently included electron-positron pair production for photons and in-flight annihilation for positrons. In addition, we have incorporated the physics described in the previous section to include the effects of multiparticle excitation. This is implemented as follows. When an inelastic collision with the outer shell occurs, we sample the cross sections for n-particle excitation for the given electron energy E to determine the number of electron-hole pairs generated at the interaction site. We subsequently sample the energy T transferred to the medium from the cumulative cross sections. This kinetic energy is assumed to be equally distributed among the n electron-hole pairs. The thermalization distance is calculated using the Knights-Davis equation. For the spur core, we assume a Gaussian distribution with a full width at half maximum given by $r=\gamma v/\omega_{pe}$, where γ is a parameter we have introduced to obtain agreement with experimental data. In our simulations, we use a value of $\gamma=1.6$.

We follow all photons, electrons, and positrons until they reach a cutoff energy E_{cut}. We use a value of $E_{cut}=50$ eV since Eq. (2) for the inelastic cross section is derived in the first Born approximation. We found that this particular energy was a threshold value above which the simulation results did not vary much. Another reason for introducing the cutoff energy is the possible inelastic collisions of low-energy electrons with phonons, the physics of which is not well understood for amorphous materials. As the electron's kinetic energy falls beyond the cutoff energy it is removed from the simulation.

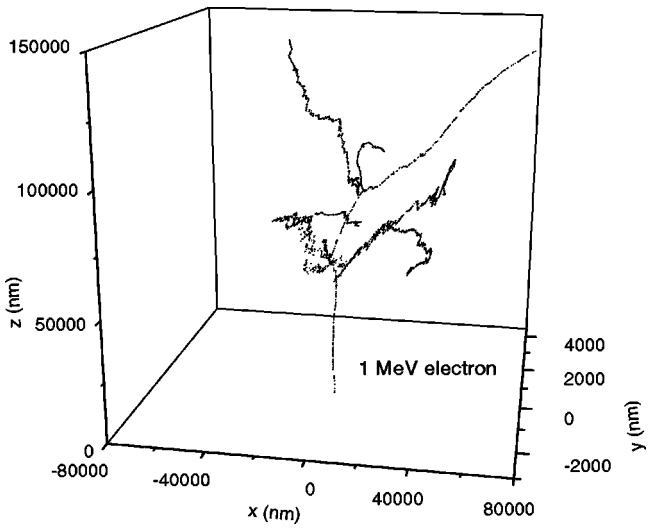

FIG. 7. Typical electron track structure for a 1 MeV electron in a-Se. The electron trajectory begins at the bottom of the figure and ends at the top.

For each inelastic outer-shell collision we record the energy deposited E_{dep} and the number of pairs created n, and calculate $W_0=E_{dep}/n$. After averaging over many histories the simulated energy required to create an electron-hole pair was found to be $W_0 \approx 4.8$ eV, which lies within the range of accepted values of $4 \leqslant W_0 \leqslant 7$ eV for a-Se.[7] Note that in Ref. 12 W_0 was taken as a parameter, whereas in this work it is determined directly from the simulations. Figure 7 shows a typical track structure for a 1 MeV electron traversing the a-Se detector. The spur core size, averaged over the track structures, is plotted versus incident photon energy in Fig. 8 for an a-Se thickness of 150 μm. As the photon energy increases, the average size of the core is seen to increase due to the higher kinetic energies of the secondary ionizing electrons produced by the primary photons. As shown in Fig. 9, the number of pairs in a spur, averaged over the track structures, increases only mildly with the incident photon energy over the range of energies shown.

Once the track structures were calculated, the subsequent dynamics of electron-hole pairs were modeled according to the many-body Smoluchowski equation

$$\frac{\partial P_i^{\pm}(\mathbf{r},t)}{\partial t} = \pm \mu_{\pm} \mathbf{E}_i \cdot \nabla P_i^{\pm}(\mathbf{r},t) + D_{\pm} \nabla^2 P_i^{\pm}(\mathbf{r},t), \quad (15)$$

where $P_i^{\pm}(\mathbf{r},t)$ denotes the probability that the ith carrier is found at the position $\mathbf{r}$ at time t, $\mathbf{E}_i$ is the total (self-consistent plus applied) electric field at the position of the ith particle, and $\mu_{\pm}$ and $D_{\pm}$ are the mobility and the diffusion

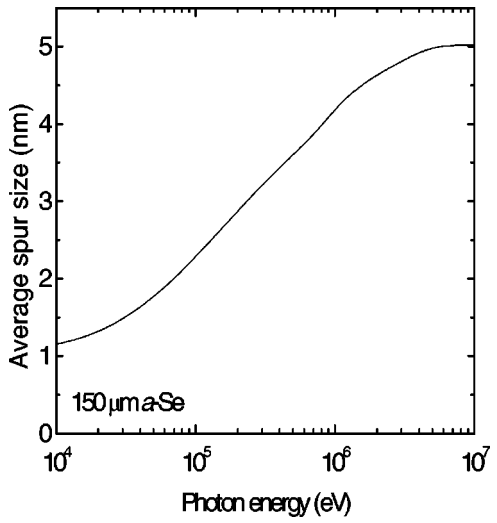

FIG. 8. Average spur core size versus photon energy. The a-Se thickness is 150 μm.

coefficients of the given carrier, respectively. This equation was solved using Monte Carlo techniques, by following the motion of the carriers through discrete time steps. The simulation code has been described elsewhere.[13] The electron-hole mobilities incorporate the effect of shallow traps present in a-Se. For electric fields above approximately 1 V/μm, the effect of deep traps is believed to be unimportant[9] and we ignored this effect in our simulations. For a given photon energy, the fraction of pairs that escape recombination η is calculated for each track structure and averaged over many histories. Subsequently the energy $W_{\pm}=W_0/\eta$ required to create a detectable electron-hole pair was calculated.

Figure 10 shows the electric field dependence of $W_{\pm}$ for three photon energies (40 keV, 140 keV, and 1.25 MeV) along with the experimental data points measured by Mah *et al.*[9] (^{60}Co) and by Blevis *et al.*[26] (40 and 140 keV). As one can see there is a good agreement between the theoretical and experimental values within uncertainties. As previously discussed, the electric field dependence is due to the fact that more particles will escape recombination with increased electric field, which will lead to higher η and lower $W_{\pm}$. The scaling with electric field, however, depends on both the number of electron-hole pairs and their spatial distribution within a spur.

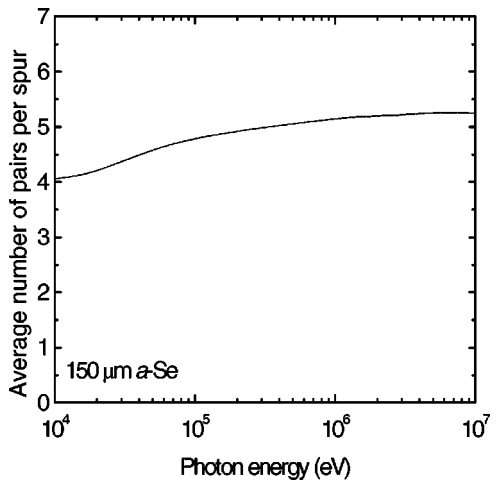

FIG. 9. Average number of electron-hole pairs in a spur versus photon energy. The a-Se thickness is 150 μm.

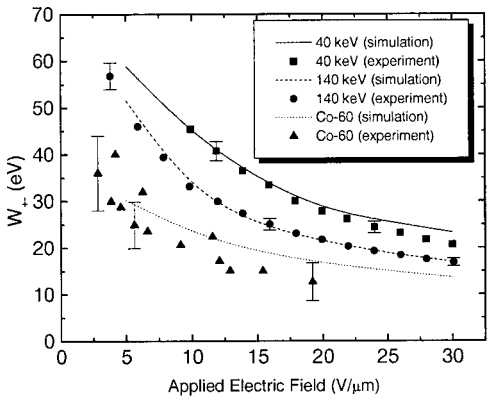

FIG. 10. The dependence of $W_{\pm}$ on the applied electric field along with experimental values measured by Blevis *et al.* (Ref. 26) and Mah *et al.* (Ref. 9). The thickness of the a-Se layer is 150 μm for the 40 and 140 keV photons, and 50 μm for the 1.25 MeV (^{60}Co) photons.

The dependence of $W_{\pm}$ on electron energy, for an applied electric field of 10 V/μm, is shown in Fig. 11. $W_{\pm}$ is seen to decrease with increasing energy and to reach a plateau at approximately 600 keV. The energy dependence is due to the fact that the spur size is proportional to the electron velocity v. As the spur size increases, electron-hole pairs are farther apart on average resulting in less recombination and a correspondingly lower $W_{\pm}$. The plateau arises because v saturates at relativistic energies.

In Fig. 11, we also show the dependence of $W_{\pm}$ on photon energy. The trend is similar to that of electrons, except that $W_{\pm}$ is higher and the plateau is reached at about 1 MeV instead of 600 keV. This occurs because the ionizing secondary electrons are of lower energy than their parent photons. Also shown in Fig. 11 are experimental values measured by

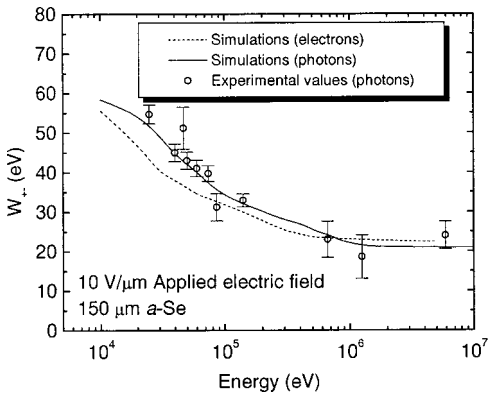

FIG. 11. The energy dependence of $W_{\pm}$ for photons (solid curve) and electrons (dashed curve). Also shown are experimental measurements by Blevis *et al.* (Ref. 26) and Mah *et al.* (Ref. 9). The thickness of the a-Se layer is 150 μm, and the applied electric field is 10 V/μm.

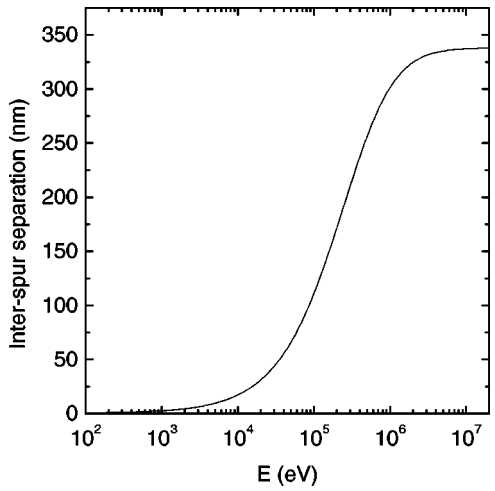

FIG. 12. The interspur separation distance ($1/N\sigma_{outer}$) plotted versus electron energy.

Mah *et al.*[9] and by Blevis *et al.*[26] The simulations agree with the measurements within experimental uncertainties.

The energy dependence of $W_{\pm}$ in a-Se have been debated by various authors for quite some time.[8,7,27] The two main competing models have been the Onsager model of geminate recombination and the Jaffe model of columnar recombination. In the Jaffe model, it is assumed that the ionizing electrons produced by x rays create electron-hole pairs continuously in a column surrounding their tracks. For this to hold the separation between spurs would have to be smaller than the spur size. The interspur separation, calculated from the total outer inelastic cross sections, is plotted in Fig. 12. Assuming that on average the spur size is 5–6 nm, the overlapping only becomes important when the electron energy is less than 5 keV. The columnar model is therefore too simplistic a model to describe recombination over a wide range of incident energies. In the Onsager model, on the other hand, it is assumed that charges can only recombine with their geminate (original) pair. This model leads to a dependence of $W_{\pm}$ on electric field, albeit not with the proper slope, but does not predict a dependence on x-ray energy. The reason for the failure of this model is twofold: first, it takes into account only a single electron-hole pair while there are on average about 4-5 pairs in a spur, and second, the distance between pairs does not vary with energy of the ionizing electron since only thermalization is taken into account, which only depends on energy *transfer*.

Our model can perhaps be seen as an extension of the Onsager theory. The model is extended to include multiple electron-hole pairs in a spur. The energy dependence of $W_{\pm}$ comes from the velocity-dependent spur size. Our results suggest that although interspur separation can influence the energy dependence, it does not play as significant a role as the size of the spur.

On a minor note, the temperature dependence of $W_{\pm}$ has sometimes been used to distinguish between recombination models. The Onsager model predicts a temperature dependence while the columnar model does not. Experimental evidence about the temperature dependence of $W_{\pm}$, however, is contradictory. Hirsch and Jahakhani[8] have found that η increases by more than a factor of 2 between 200 and 300 K, while recent measurements by Haugen *et al.*[28] have shown that there is no temperature dependence in the range 260–300 K. We have run simulations for various temperatures with our code and have found no significant dependence (less than 5%) within 200–300 K. Further experimental evidence must be acquired before the temperature dependence can be properly understood.

V. CONCLUSIONS

The signal generated by x rays in the photoconductor a-Se is not well understood. It is primarily governed by recombination, which is very sensitive to the positions of the electron-hole pairs generated along the photon/electron/positron track structures. In this work, we develop a theoretical description of the charge formation in a-Se. In our model, high-energy electrons created by the interacting x rays undergo interactions with atomic electrons, exciting collective (plasma) oscillations as well as single electron-hole pairs. We develop cross sections for the decay of plasma oscillations into the creation of n electron-hole pairs. These cross sections are integrated into a Monte Carlo code that simulates the stochastic track structures in a-Se. From these tracks, we determine the initial positions of electrons and holes in the medium. We subsequently follow their time evolution using a simulation code that effectively solves the many-body Smoluchowski equation. From these simulations we calculate $W_{\pm}$ which depends on both the pair creation energy W_0 and the escape efficiency η. Using our model, we calculate $W_{\pm}$ as a function of incident energy and electric field for both electrons and photons. We compare to available experimental data and show good agreement. $W_{\pm}$ decreases with electric field because a higher fraction of particles escape recombination, thus increasing η. $W_{\pm}$ decreases with increasing photon energy up to about 1 MeV, after which it reaches a constant plateau. In another paper[9] this has been qualitatively described by a interspur recombination mechanism. In our model, the energy dependence is not due to interspur recombination since spurs are only close enough to affect each other at energies less than about 5 keV. Instead, the energy dependence is attributed to an energy-dependent spur size. This arises because energy is deposited within a sphere whose size is proportional to the incident velocity of the ionizing particle. The escape efficiency increases with increasing spur size because electron-hole pairs in the spur are farther apart, resulting in a greater probability of escaping recombination. This mechanism seems to explain the observed energy dependence of $W_{\pm}$ in a-Se. The results presented in this paper can be used to calculate the signal in a-Se based x-ray detectors for applications in diagnostic radiology and portal imaging. Better understanding of the signal generation in these detectors may lead to further optimization of both detector design and the choice of x-ray energy spectra used for imaging with these detectors.

ACKNOWLEDGMENTS

This research is partly supported by a Natural Science and Engineering Research Council of Canada (NSERC) University Industry Grant (CRD 215792-98).

[1] J. Rowlands and S. Kasap, Phys. Today **50**(11), 24 (1997).
[2] J.A. Rowlands and D.M. Hunter, Med. Phys. **22**, 1983 (1995).
[3] W. Zhao and J.A. Rowlands, Med. Phys. **24**, 1819 (1997).
[4] W. Zhao and J.A. Rowlands, Med. Phys. **22**, 1595 (1995).
[5] T. Falco, H. Wang, and B.G. Fallone, Med. Phys. **25**, 814 (1998).
[6] W. Que and J.A. Rowlands, Med. Phys. **4**, 365 (1995).
[7] W. Que and J.A. Rowlands, Phys. Rev. B **51**, 10 500 (1995).
[8] J. Hirsch and H. Jahankhani, J. Phys.: Condens. Matter **1**, 8789 (1989).
[9] D. Mah, J.A. Rowlands, and J.A. Rawlinson, Med. Phys. **25**, 444 (1998).
[10] A. Chatterjee, *Radiation Chemistry: Principles and Applications*, edited by Fahataziz and M. Rodgers (VCH, New York, 1987), p. 9.
[11] A. Chatterjee and W. Holley, Adv. Rad. Biology **17**, 181 (1993).
[12] M. Lachaine and B.G. Fallone, J. Phys. D **33**, 551 (2000).
[13] M. Lachaine and B.G. Fallone, J. Phys. D **33**, 1417 (2000).
[14] J. Lindhard, K. Dan. Vidensk. Selsk. Mat. Fys. Medd. **28**(8), 1 (1954).
[15] R.H. Ritchie, Phys. Rev. **114**, 644 (1959).
[16] H.H. Rossi and M. Zaider, *Microdosimetry and its Applications* (Springer, New York, 1995).
[17] W. Jones and N. March, *Theoretical Solid State Physics* (Dover, New York, 1973), Vol. 1.
[18] M.G. Bell and W.Y. Liang, in *Proceedings of the 5th International Conference on Amorphous and Liquid Semiconductors*, edited by G. Stuke and W. Brenig (Taylor and Frances, London, 1973), p. 1385.
[19] N. March and M. Parrinello, *Collective Effects in Solids and Liquids* (Hilger, Bristol, 1982).
[20] R.H. Ritchie and W. Brandt, in *Radiation Research:Biomedical, Chemical and Physical Perspectives*, edited by O.F. Nygaard, H.I. Adler, and W.K. Sinclair (Academic Press, New York, 1975), p. 315.
[21] R.H. Hamm *et al.*, Radiat. Res. **104**, 5 (1985).
[22] J.C. Ashley and M.W. Williams, Rome Air Development Center, Griffiss Air Force Base, New York, Report No. RADC-TR-83-87, 1983 (unpublished).
[23] N. Bohr, Mat. Fys. Medd. K. Dan. Vidensk. Selsk. **18**, 1 (1948).
[24] W. Brandt and R.H. Ritchie, in *Physical Mechanisms in Radiation Biology*, edited by R.D. Cooper and R.W. Wood (United States Atomic Energy Commission, Oak Ridge, TN, 1974), p. 315.
[25] J.C. Knights and E.A. Davis, J. Phys. Chem. Solids **35**, 543 (1975).
[26] I.M. Blevis, D.C. Hunt, and J.A. Rowlands, J. Appl. Phys. **85**, 7958 (1999).
[27] C.A. Klein, J. Appl. Phys. **39**, 2029 (1968).
[28] C. Haugen, S.O. Kasap, and J. Rowlands, J. Phys. D **32**, 200 (1999).